International Journal of Geo-Information

MDPI

Article

Landscape Risk Assessment of Ancient Sites Using PSR Framework: A Case Study of Yuncheng, China (1990–2024)

Yinglian Gao [1,2], Wei Hua [3,*], Beibei Zhao [1,2], Binhao Du [1,2], Zhenhua Gao [4,5] and Miaole Hou [1,2,6]

1 School of Geomatics and Urban Spatial Informatics, Beijing University of Civil Engineering and Architecture, Beijing 102616, China; houmiaole@bucea.edu.cn (M.H.)
2 Key Laboratory for Architectural Heritage Fine Reconstruction & Health Monitoring, Beijing 100044, China
3 National Institute of Natural Hazard, Ministry of Emergency Management of the People's Republic of China, Beijing 100085, China
4 Shanxi Provincial Research Institute of Archaeology, Taiyuan 030001, China
5 Shanxi Key Laboratory of Scientific and Technological Archaeology, Taiyuan 030001, China
6 Institute of Digital and Intelligent Preservation and Inheritance of Cultural Relics, Chang'an University, Xi'an 710064, China
* Correspondence: huawei@ninhm.ac.cn

Abstract

Ancient sites are vulnerable cultural heritage assets that are increasingly threatened by climate change, natural erosion, and anthropogenic pressures, posing significant challenges to the stability and integrity of their landscapes. Therefore, the identification and systematic assessment of landscape risks at ancient sites are essential for preventive conservation and sustainable landscape management. To address the limitations of risk assessment and long-term dynamic risk analysis of landscape risks at ancient sites, this study develops a landscape risk assessment indicator system based on the Pressure-State-Response (PSR) framework, incorporating three dimensions: natural environment, human activities, and site protection. The entropy weight method was employed to determine indicator weights from the relative dispersion of the standardized indicators. From a landscape-scale perspective, this study systematically analyses the landscape risk of ancient sites in Yuncheng City from 1990 to 2024. The results indicate the following: (1) The landscape risk of ancient sites in Yuncheng exhibits significant spatial heterogeneity. Very high, high, and medium risk levels are primarily distributed in the foothill transition zone, while low and very low risk levels are mainly found in the inland plain areas. This spatial differentiation remained generally stable throughout the study period. (2) The landscape risks associated with ancient sites in Yuncheng City exhibit significant positive spatial autocorrelation and clustering characteristics, and their clustering structure remained relatively stable throughout the study period. (3) The overall risk structure is dominated by low to medium risk levels, with risk-level transitions occurring primarily between adjacent levels in both directions. During the later stage of the study period, the risk structure showed a shift toward medium and high risk levels. The findings provide a scientific basis for risk management and the sustainable development of regional ancient site landscapes.

Keywords: ancient sites; landscape risk; spatiotemporal analysis; cultural heritage; PSR

Check for updates

Academic Editors: Wolfgang Kainz and Godwin Yeboah

Received: 10 June 2026
Revised: 2 September 2026
Accepted: 29 September 2026
Published: 1 October 2026

Copyright: © 2026 by the authors. Published by MDPI on behalf of the International Society for Photogrammetry and Remote Sensing. Licensee MDPI, Basel, Switzerland. This article is an open access article distributed under the terms and conditions of the Creative Commons Attribution (CC BY) license.

1. Introduction

Cultural heritage embodies historical, artistic, scientific, and social values and represents a non-renewable resource [1]. As an important category of cultural heritage, ancient

sites are non-renewable and highly vulnerable assets [2]. Once damaged, they are often difficult or impossible to restore. The value and significance of ancient sites are often closely linked to their surrounding landscape environment [3]. The stability and overall integrity of the landscape directly affect the preservation condition and evolutionary process of ancient sites. Therefore, the protection of ancient sites should extend beyond the preservation of individual sites to encompass the integrated conservation of their surrounding landscape systems.

Against the backdrop of accelerating global climate change, the frequency and intensity of extreme weather events are increasing. In combination with sudden-onset natural hazards, including earthquakes, floods, and landslides, these changes pose significant threats to ancient sites and their surrounding landscapes [4–6]. Meanwhile, long-term ecological changes, such as vegetation degradation and soil erosion, also threaten the stability of ancient site landscapes [7,8]. In addition, human activities such as urban expansion and the development of cultural tourism have continuously intensified, placing significant pressure on the surrounding landscapes of ancient sites [9]. Under the combined influence of natural processes and anthropogenic activities, ancient site landscapes are facing increasingly prominent risks.

In this study, landscape risk refers to the overall risk of deterioration in the landscape integrity, stability, and long-term preservation capacity of ancient sites resulting from the combined effects of changes in the natural environment, human disturbances, and variations in conservation management capacity. In recent years, scholars have increasingly focused on the dynamics of cultural heritage landscapes and methods for assessing associated risks. Regarding landscape changes, scholars have examined land-use/land-cover changes, the evolution of landscape pattern and their driving mechanisms, and land-use changes within cultural heritage sites [10–14]. In terms of risk assessment, some studies have adopted a landscape ecological risk perspective to quantitatively assess world cultural heritage sites and typical areas [15,16]. Canesi et al. conducted a heritage risk and vulnerability assessment of the Wachau World Agricultural Cultural Landscape in Austria, focusing on climate-related stresses such as extreme rainfall and flooding [17]. Regarding the landscape risks of ancient sites, most studies have focused on typical areas. Li et al. focused on city sites in the Central Plains region and developed a landscape risk assessment system based on changes in land cover, identifying threats to these sites from a cultural heritage landscape perspective [18]; Zhang et al. developed a comprehensive assessment framework integrating K-means clustering and the entropy weight method to quantitatively evaluate regional environmental risks at the Xinjiang Great Wall site [19]. Zengin et al. assessed the risks posed by sea-level rise to archaeological and historical sites along the Mediterranean coast [20]. Peruzzo et al. focused on geological and cultural heritage sites and employed a two-tier risk assessment method to evaluate the effects of infrastructure development, agricultural expansion, and other threats on landscape integrity and geological diversity [21]. However, existing studies are largely limited to single cultural heritage assessments or large-scale regional environmental risk assessments. Few studies have explicitly defined site-centered landscape units and applied a unified indicator framework to systematically analyze their long-term risk dynamics.

The Pressure-State-Response (PSR) framework was originally proposed by Canadian statisticians Rapport and Friend [22]. It provides a systematic approach to characterizing the interactions between human activities and environmental changes and has now been widely applied in various fields. In ecological risk assessment, the PSR framework has been used to quantitatively assess ecological risks in various scenarios, including islands, wetlands, and arid regions [23–27]. In ecological security assessment, it has been applied to evaluate ecological security at different spatial scales [28–30]. Additionally, this framework has

been effectively applied in regional ecological and environmental quality assessment [31], wetland environmental risk analysis [32], and sustainable urban resource assessment [33]. In recent years, some studies have begun to explore the application of the PSR framework to the field of cultural heritage conservation. Using traditional villages in Hunan Province as a case study, Zhong et al. developed a PSR-based assessment system for human habitation suitability, providing a scientific basis for the conservation and sustainable development of these villages [34]; Fu et al. developed a flood risk assessment method integrating the PSR framework with game theory and the Cloud model to quantitatively assess flood risks to urban cultural heritage [35]; Bai et al. proposed a framework integrating the DPSIR model with the extended cloud model to assess typhoon-related risks to coastal architectural heritage [36]. In summary, the PSR framework provides an effective method for risk assessment, but its application in the field of cultural heritage remains relatively limited. For ancient sites in particular, systematic quantitative assessments of the coupled effects of changes in the surrounding natural environment, human activities, and site conservation remain scarce.

Therefore, developing a scientific, systematic, and comparable assessment index system integrating the dimensions of the natural environment, human activities, and site protection, and conducting landscape-scale risk assessments and long-term dynamic analyses of ancient sites, remain important research priorities.

This study takes Yuncheng City as the study area and develops a landscape risk assessment method for ancient sites based on the PSR framework, integrating indicators related to the natural environment, human activities, and site protection. This method enables the quantitative identification of landscape risks to ancient sites. Using this method, the study systematically analyzes the characteristics of landscape risk changes in Yuncheng's ancient sites since 1990. The study aims to address the existing gaps in ancient site landscape risk assessment and long-term dynamic analysis, providing a scientific basis and technical reference for the preventive conservation, refined management, and sustainable development of ancient sites in Yuncheng City. The main contributions of this study are as follows:

(1) Based on the PSR framework, this study developed an indicator system for assessing landscape risks at ancient sites, incorporating indicators across three dimensions: the natural environment, human activities, and site protection. The system enables the quantitative assessment of landscape risks at ancient sites.
(2) In terms of spatial scale, this study adopts a landscape-scale approach for ancient sites, incorporating both the sites and their surrounding landscape environments into a unified analytical unit. This approach addresses the limitation of previous studies that paid insufficient attention to the landscapes surrounding the sites.
(3) Using multi-source long-term time-series data from 1990 to 2024, this study assesses the landscape risks at ancient sites in Yuncheng City and reveals the spatiotemporal evolution of these risks. The findings provide a scientific basis for the protection and sustainable development of the ancient site landscapes.

2. Materials and Methods

2.1. Overview of the Study Area

Yuncheng City (110°15′–112°04′ E, 34°35′–35°49′ N) is located in the Jinnan Basin in southern Shanxi Province, China. The study area generally features a topography that is higher in the northeast and lower in the southwest, with diverse terrain and landforms, including an interlaced distribution of mountains, hills, and plains [37]. The region is influenced by monsoon activity throughout the year and has a warm-temperate continental monsoon climate, characterized by cold, dry winters and hot, rainy summers [38]. In addition, this region is located in the Loess Plateau in western China and is one of the

areas in China most prone to geological disasters [39]. These natural conditions, combined with anthropogenic disturbances such as urban expansion, agricultural development, and cultural tourism activities, have intensified interactions between the natural factors and human activities, thereby posing multiple risks to the safety of ancient site landscapes. The coexistence of piedmont zones, alluvial plains, dense archaeological distributions, and rapidly changing land use makes Yuncheng a suitable test area for regional heritage landscape-risk assessment. Figure 1 shows a general map of the study area.

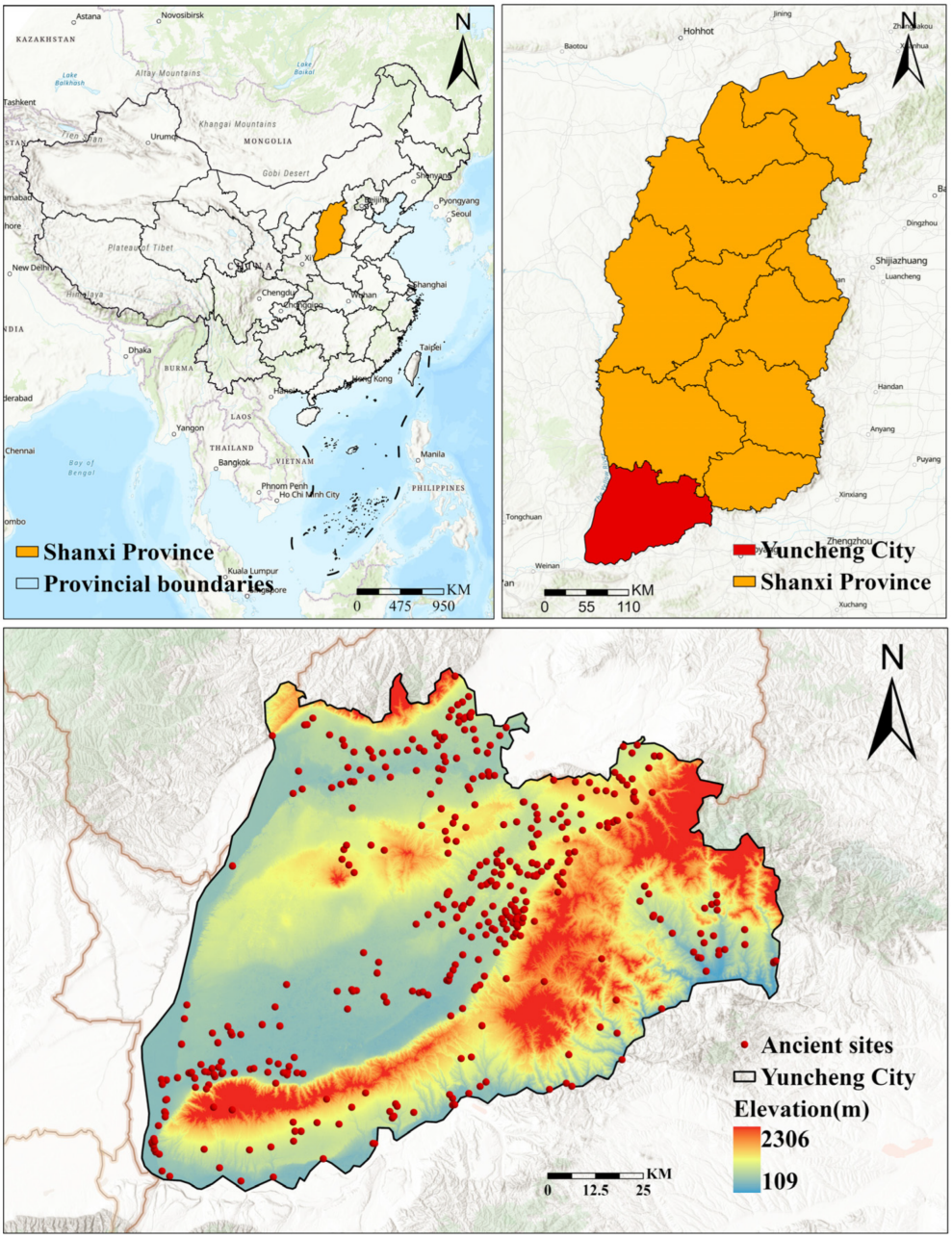


Figure 1. Overview map of the study area.

2.2. Data Sources and Preprocessing

2.2.1. Ancient Sites Data

Data and information on ancient sites were primarily sourced from the Third Cultural Relics Survey of Yuncheng City, Shanxi Province, totaling 1912 ancient sites. The data include details such as location, area size, and site type. This study selected a total of 445 sites, comprising national key cultural relics protection units, provincial cultural relics

protection units, and municipal/county-level cultural relics protection units. Considering spatial form differences and research applicability, 432 point-type and area-type ancient site samples were selected. After excluding 27 sites with missing area information, the remaining 405 sites were used for the landscape risk analysis.

2.2.2. Remote Sensing Image Dataset

The remote sensing data used in this study were obtained from the "China Earth Observation Data Cube: The 30-m Seamless Annual Leaf-On Landsat Composites from 1985 to 2024" dataset developed by Central South University [40]. This dataset provides annual 30-m Landsat growing-season composite imagery covering the period from 1985 to 2024. According to the dataset documentation, these products have undergone standardized preprocessing procedures, including cross-sensor spectral harmonization, cloud and cloud-shadow masking, and annual compositing. The Normalized Difference Vegetation Index (NDVI) was calculated for each year using the Google Earth Engine platform based on the annual leaf-on Landsat composites. The derived NDVI values characterize the integrated vegetation conditions during the annual leaf-on growing season.

2.2.3. Meteorological Datasets

Temperature and precipitation data were obtained from the "1-km monthly mean temperature dataset for China (1901–2024)" and the "1-km monthly precipitation dataset for China (1901–2024)" published by National Tibetan Plateau/Third Pole Environment Data Center [41]. These datasets have a spatial resolution of 0.0083333° (approximately 1 km), with units of 0.1 °C and 0.1 mm, respectively. Based on these datasets, this study calculated annual precipitation and annual average temperature.

2.2.4. Land Cover Dataset

Land cover data were obtained from the China Land Cover Data (CLCD) dataset [42] released by Wuhan University, with a spatial resolution of 30 m × 30 m, covering land cover information from 1985 and 1990–2024. This study selected land cover data from eight time periods: 1990, 1995, 2000, 2005, 2010, 2015, 2020, and 2024.

2.2.5. Population Dataset

The population dataset used were the Globpop dataset released by Beijing Normal University [43] and the LandScan Global 2024 dataset developed by the Oak Ridge National Laboratory [44]. The Globpop dataset contains population numbers and population density from 1990 to 2022, with a spatial resolution of 30 arc seconds (approximately 1 km). The LandScan dataset provides spatial population distribution data for 2024, with a spatial resolution of 30 arc seconds (approximately 1 km). This study selected the population data from seven periods (1990, 1995, 2000, 2005, 2010, 2015, and 2020) in the Globpop dataset, and supplements the 2024 data from LandScan to ensure the consistency of the research time scale.

2.2.6. Digital Elevation Model Data

The Digital Elevation Model (DEM) data were derived from the ASTER GDEM data published on the Geospatial Data Cloud Platform [45], with a spatial resolution of 30 m.

To address the spatiotemporal inconsistencies among the multi-source data (Table 1), this study preprocessed the data using ArcGIS Pro 3.0.2. First, all data were projected to a common coordinate reference system, WGS 1984 UTM Zone 49N. Next, the study area boundary was used to define the clipping extent, and all raster datasets were clipped to a uniform spatial extent to improve computational efficiency.

Table 1. Summary of data sources.

Dataset	Spatial Resolution	Temporal Coverage	File Format	Sources
Ancient sites data	/	/	.xls	The Third National Cultural Relics Census
China Earth Observation Data Cube: The 30-m Seamless Annual Leaf-On Landsat Composites from 1985 to 2024	30 m × 30 m	1985–2024	.tif	https://zenodo.org/records/14131869 (accessed on 15 April 2026)
1-km monthly mean temperature dataset for China (1901–2024)	1 km × 1 km	1901–2024	.nc	https://doi.org/10.11888/Meteoro.tpdc.270961
1-km monthly precipitation dataset for China (1901–2024)	1 km × 1 km	1901–2024	.nc	https://doi.org/10.5281/zenodo.3114194
China Land Cover Dataset	30 m × 30 m	1985, 1990–2024	.tif	https://zenodo.org/records/15853565 (accessed on 14 April 2026)
Globpop Dataset	1 km × 1 km	1990–2022	.tif	https://zenodo.org/records/11179644 (accessed on 15 April 2026)
LandScan Global 2024 Dataset	1 km × 1 km	2024	.tif	https://doi.org/10.48690/1532445
ASTER GDEM	30 m × 30 m	/	.img	http://www.Gscloud.cn (accessed on 14 April 2026)

2.3. Methods

This study first developed an indicator system for assessing landscape risks at ancient sites based on the PSR framework, comprising three dimensions: the natural environment, human activities, and site protection. Second, the entropy weight method was employed to determine the weight of each indicator. Finally, the assessment method was applied to evaluate landscape risks at ancient sites in Yuncheng City, identifying the spatiotemporal variations and changes in risk levels, and further reveal spatial clustering patterns of risks through spatial autocorrelation analysis. The technical workflow is shown in Figure 2.

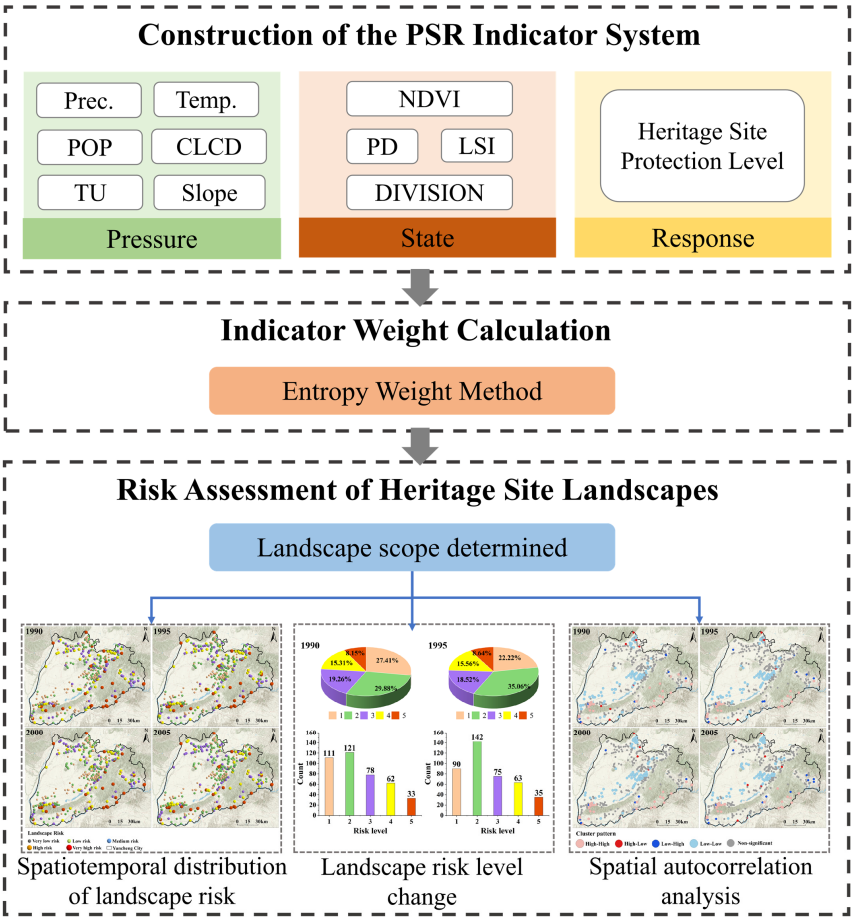


Figure 2. Technology roadmap.

2.3.1. Determination of the Analysis Units

(1) Determining the threshold for the minimum landscape analysis area

Landscape risks at ancient sites depend not only on conditions within the sites themselves but also on environmental changes and human disturbances in their surrounding areas. Therefore, the determination of landscape analysis units requires consideration of both the scale characteristics of the ancient site and the representativeness of their surrounding landscapes. An analysis of the areas of 405 ancient sites showed that 378 sites had areas smaller than 1,000,000 m^2, accounting for approximately 93% of all sites. Further analysis revealed that approximately 83% of the ancient sites with areas smaller than 1,000,000 m^2 had areas below 200,000 m^2, indicating that most ancient sites in the study area are generally small in size. To ensure sufficient landscape coverage for small ancient sites while preserving the actual spatial characteristics of larger sites, this study adopted the method proposed in previous research [18]. Specifically, 1,000,000 m^2 was set as the threshold for determining the landscape analysis area. For sites smaller than this threshold, 1,000,000 m^2 was used as the reference area for calculating the equivalent landscape analysis radius, whereas the actual site area was used for larger sites.

(2) Development of the landscape analysis unit

To adequately represent the spatial influence of ancient sites and their surrounding environments, an equivalent landscape radius was first calculated based on the area of each site. This radius was used to define the corresponding landscape analysis extent. Considering the compatibility of raster data with regular spatial units, the circumscribed square of the equivalent circular (with a side length of 2r) was adopted as the final landscape analysis unit [18]. The formula for calculating the equivalent landscape radius is as follows:

$$r_i = k\sqrt{\frac{S_i}{\pi}} \quad (1)$$

Here, r_i represents the landscape radius of the i-th ancient site (m), S_i represents the area of the corresponding site (m^2), and k represents the scale adjustment coefficient. If $k < 1$, the landscape analysis unit may be insufficient to encompass the site and its surrounding environment, whereas excessively large values of k may lead to substantial spatial overlap and redundancy among analysis units. Drawing on the scale adjustment coefficients used in previous studies of landscape risk assessment for ancient sites [18], this study sets $k = 1.5$. This value can encompass the potential disturbance areas around the sites while reducing the spatial overlap among different analysis units, thereby improving the stability and comparability of the spatial analysis results.

To assess the sensitivity of the results to the selection of spatial analysis parameters and unit shapes, this study conducted a sensitivity analysis. Specifically, the minimum area threshold, scale adjustment coefficient, and spatial analysis unit shape (circular or square) were varied to evaluate the consistency of the risk assessment results under different settings. Consistency was assessed using Spearman's rank correlation coefficient, the number of ancient sites whose risk levels remained unchanged, and the overlap rate of the top 20% of high-risk sites. The robustness of the assessment results under different spatial analysis settings is further discussed in the Discussion section.

2.3.2. Development of a Landscape Risk Assessment Indicator System for Ancient Sites Based on the PSR Framework

Landscape risks at ancient sites are influenced by complex factors, including human disturbances and changes in the natural environment. Based on the PSR framework, this study develops a landscape risk assessment index system for ancient sites from three di-

mensions: landscape risk pressures, landscape states, and protection response capacity. The "Pressure" dimension characterizes external disturbances and environmental constraints affecting ancient-site landscapes, including climate change, human disturbance, and natural contextual conditions such as topography. The "State" dimension describes the existing landscape structure and environmental conditions resulting from these external pressures; and the "Response" dimension characterizes the existing institutional protection status and potential risk intervention capacity of ancient sites, primarily reflecting the stability of their protection and management foundation.

This study developed a preliminary indicator system comprising 13 indicators to assess landscape risks at ancient sites, and conducted multicollinearity tests using the Variance Inflation Factor (VIF) and tolerance (TOL) values. The formulas for calculating VIF and TOL are as follows:

$$VIF_j = \frac{1}{\left(1 - R_j^2\right)} \tag{2}$$

$$TOL_j = \frac{1}{VIF_j} \tag{3}$$

Here, R_j^2 represents the coefficient of determination for the jth independent variable with respect to all other independent variables, and the TOL value is the reciprocal of the VIF value.

The initial multicollinearity analysis indicated that the VIF values for NDMI, NDVI, and SHDI were relatively high (VIF > 10), suggesting potential multicollinearity among some indicators. Given that NDVI is widely used in remote sensing-based ecological monitoring and can effectively characterize regional vegetation conditions, NDVI was retained as an ecological status indicator, while NDMI was excluded. In addition, SHDI was excluded because of its strong correlation with other landscape pattern indicators. Following this screening process, the remaining indicators were subjected to a second multicollinearity assessment. All VIF values were below 7, while all TOL values exceeded 0.1 (Table 2), indicating the absence of substantial multicollinearity among the retained indicators. Ultimately, an 11-indicator assessment system for landscape risks at ancient sites was established (Table 3).

(1) Pressure layer

In the pressure layer, six indicators—precipitation, temperature, terrain undulation, slope, land cover, and population—were selected to characterize the intensity of external pressures and environmental constraints on the landscape of ancient sites.

Table 2. Results of the multicollinearity test.

Indicators	Variance Inflation Factor (VIF)	Tolerance (TOL)
Slope	6.25	0.16
Terrain undulation	4.98	0.20
LSI	4.05	0.25
Land cover	3.20	0.31
PD	3.17	0.32
DIVISION	2.32	0.43
NDVI	1.84	0.54
Temperature	1.80	0.56
Precipitation	1.74	0.57
Population	1.45	0.69
Protection level	1.08	0.92

Table 3. Indicator system for landscape risk assessment of ancient sites.

Guideline	Element	No.	Indicator	Factor Type
Pressure	Climate	1	Precipitation	Positive
		2	Temperature	Positive
	Geological	3	Terrain undulation	Positive
		4	Slope	Positive
	Human activities	5	Land cover	Positive
		6	Population	Positive
State	Environment	7	NDVI	Negative
	Landscape pattern	8	LSI	Positive
		9	DIVISION	Positive
		10	PD	Positive
Response	Preservation	11	Protection level	Negative

Temperature and precipitation are major environmental threats to cultural heritage [46]. Temperature affects the landscapes of ancient sites by influencing moisture conditions, soil moisture, and freeze–thaw cycles [47,48], while precipitation affects landscape stability through surface runoff, soil erosion, and vegetation conditions [49,50]. In this study, area-weighted annual mean temperature and cumulative annual precipitation within each landscape analysis unit were used to characterize the climatic background pressure with these two factors. Although moderate precipitation and suitable temperatures may provide ecological buffering, extreme climatic conditions can intensify environmental disturbances. Thus, their relationships with landscape risk may be non-monotonic. Based on the general direction of the potential impact of temperature and precipitation on landscape risk, the two were both assigned as positive indicators to represent overall regional climatic pressure rather than to imply a direct or monotonic marginal effect on landscape risk. Terrain undulation and slope are static topographic conditions that represent elevation variability and terrain inclination, respectively. They may indirectly influence landscape risk by affecting runoff, soil erosion, and surface stability [51]. Therefore, both indicators were treated as positive indicators, with higher values indicating greater potential landscape risk. These two indicators were derived from the DEM and slope calculated as the mean grid-cell values within each landscape analysis unit.

The formula for calculating terrain undulation is as follows:

$$TU = H_{max} - H_{min} \tag{4}$$

TU stands for terrain undulation, H_{max} represents the maximum elevation within each site landscape analysis unit, and H_{min} represents the minimum elevation within each site landscape analysis unit.

Population size was used to characterize the intensity of human activity in a region. Larger populations are generally associated with more intensive construction, development, and transportation activities, thereby increasing human disturbance pressure on ancient-site landscapes [52]. In this study, the area-weighted population within each landscape analysis unit was calculated and used as the indicator value, with higher values indicating greater landscape risk. Land cover was used to characterize the extent of human-induced disturbance to landscape ecosystems [53]. Referring to previous studies, different land-cover types were assigned risk scores according to their levels of human disturbance [54]. Impervious surfaces, cropland, barren, grassland and shrub, and forest and water were assigned scores of 5, 4, 3, 2, and 1, respectively. These scores were subsequently used to

construct a land-cover risk index. To account for the potential subjectivity of the ordinal scoring scheme, a sensitivity analysis was conducted to evaluate the robustness of the results under alternative assignment schemes.

The formula for calculating the land cover risk index is as follows:

$$RI = \sum_{i=1}^{n} \left(\frac{A_i}{A} \times L_i \right) \tag{5}$$

RI denotes the land cover risk index, A_i denotes the area of the i-th land cover type within the ancient site landscape analysis unit, A denotes the total area of the ancient site landscape analysis unit, L_i denotes the risk index corresponding to the i-th land cover type, and n denotes the number of land cover types.

(2) State layer

In the state layer, four indicators—the Normalized Difference Vegetation Index (NDVI), the Landscape Shape Index (LSI), Landscape Divisibility (DIVISION), and Patch Density (PD)—were selected to comprehensively characterize the existing structural and ecological conditions of the ancient-site landscape.

NDVI was used to characterize the vegetation conditions within the landscape analysis units. Higher NDVI values generally indicate better vegetation conditions, which can enhance soil and water conservation capacity and reduces soil erosion, thereby contributing to landscape stability at ancient sites [55]. Although excessively high vegetation density may cause root-related disturbances, suggesting that the relationship between vegetation and landscape risk may be non-monotonic under certain conditions, the overall relationship at the regional scale is considered to be predominantly negative. Therefore, NDVI was treated as a negative indicator, with higher NDVI values corresponding to lower risk scores. The formula for NDVI is as follows:

$$NDVI = \frac{NIR - Red}{NIR + Red} \tag{6}$$

Here, *NIR* refers to reflectance in the near-infrared band, and *Red* refers to reflectance in the red band. The indicator value was calculated as the mean value within the analysis unit.

LSI characterizes patch-shape complexity and the regularity of landscape boundaries. DIVISION reflects the degree of landscape fragmentation, with higher values indicating greater fragmentation and generally lower landscape connectivity. PD represents the number of patches per unit area and is widely used as an indicator of landscape fragmentation. Higher values of these indicators generally indicate greater boundary complexity or landscape fragmentation, which may potentially weaken ecological buffering capacity and increase landscape risks at ancient sites. Accordingly, all three indicators were treated as positive indicators. Using FRAGTATS 4.2, annual values of these indicators were calculated for all 405 landscape analysis units from 1990 to 2024. Land cover was classified using the original seven-class CLCD classification scheme, with an 8-neighbor connectivity rule applied. The edge depth function was not enabled, and no minimum patch area threshold was imposed.

(3) Response layer

In the response layer, the protection level of ancient sites recorded in the Third National Cultural Relics Census was selected to represent protection response capability. This indicator mainly reflects the institutional protection status and potential capacity for risk intervention at ancient sites. It was used as a relatively stable proxy for institutional responses, rather than as a measure of dynamic protection responses at specific historical time points. The protection levels for ancient sites in China are primarily categorized as

national key cultural relics protection units, provincial cultural relics protection units, and municipal/county-level cultural relics protection units [56]. Higher protection levels generally correspond to more comprehensive management systems, greater financial support, and more extensive monitoring resources [57,58]. In this study, an ordinal scoring scheme was adopted to differentiate protection levels (Table 4). The protection level was treated as a negative indicator, with higher scores indicating stronger conservation capacity and lower landscape risk.

Table 4. Ancient site protection levels index.

Protection Level	Value
National key cultural relics protection units	5
Provincial cultural relics protection units	3
Municipal/county-level cultural relics protection units	1

2.3.3. Entropy Weight Method

The entropy weight method was used to derive weights based on the relative dispersion of the standardized indicators. The method determines the information contribution of each indicator according to its entropy value: indicators with greater variability contain more information and therefore contribute more to the comprehensive evaluation, resulting in higher weights [19,59–61]. This study integrated the indicator values for 405 ancient sites across eight years (a total of 3240 observations). The entropy weight method was applied to the pooled dataset to derive a single, common weight for each indicator. These common weights were then applied consistently to calculate the landscape risk index for each ancient site in each year. The calculation process is as follows:

(1) Standardize different indicators using the range-normalization method:

Positive indicators:

$$y_{ij} = \frac{x_{ij} - min(x_{1j}, x_{2j}, \ldots, x_{nj})}{max(x_{1j}, x_{2j}, \ldots, x_{nj}) - min(x_{1j}, x_{2j}, \ldots, x_{nj})} \quad (7)$$

Negative indicators:

$$y_{ij} = \frac{max(x_{1j}, x_{2j}, \ldots, x_{nj}) - x_{ij}}{max(x_{1j}, x_{2j}, \ldots, x_{nj}) - min(x_{1j}, x_{2j}, \ldots, x_{nj})} \quad (8)$$

In the formula, y_{ij} represents the standardized value of the data indicator, x_{ij} represents the raw value of the j-th indicator for the i-th observation, $max(x_{1j}, x_{2j}, \ldots, x_{nj})$ denotes the maximum value of the j-th indicator, and $min(x_{1j}, x_{2j}, \ldots, x_{nj})$ denotes the minimum value of the j-th indicator.

(2) Calculate the proportion of each sample value for each indicator:

Calculate the percentage of the value of the i-th observation within the j-th indicator relative to the total value of that indicator:

$$p_{ij} = \frac{y_{ij}}{\sum_{i=1}^{n} y_{ij}} \quad (9)$$

(3) Calculate the information entropy of the j-th indicator:

$$e_j = -\frac{1}{lnn} \sum_{i=1}^{n} (p_{ij} lnp_{ij}) \quad (10)$$

In the formula, e_j represents the entropy of the j-th indicator, and n is the total number of observations. For $p_{ij} = 0$, the term $p_{ij} ln p_{ij}$ is assigned a value of 0.

(4) Calculate the entropy weight for the j-th indicator:

$$W_j = \frac{1 - e_j}{\sum_{j=1}^{m} (1 - e_j)} \tag{11}$$

In the formula, W_j is the weight of the j-th indicator, and m is the total number of assessment indicators.

2.3.4. Risk Analysis

(1) Risk calculation

To comprehensively assess the landscape risk of ancient sites, a comprehensive risk index was constructed based on the standardized indicator values and their corresponding weights. The index represents the overall risk level of each ancient-site landscape, and risk levels were subsequently classified according to the resulting index values.

Based on the weights assigned to each indicator and the standardized results, the risk values for each site are calculated using a weighted sum method, as expressed below:

$$R_i = \sum_{j=1}^{m} W_j \cdot y_{ij} \tag{12}$$

In the formula, R_i represents the comprehensive risk index of the i-th site, W_j represents the weight of the j-th indicator, y_{ij} represents the standardized indicator value, and m represents the number of indicators.

(2) Risk classification

In this study, the Jenks natural breaks method was used to classify landscape risk at ancient sites into five levels, very low, low, medium, high, and very high. The method identifies natural groupings in the data by minimizing within-class variance and maximizing between-class variance [62]. To ensure comparability of risk levels across different years, this study integrated the risk values for 405 ancient sites across eight years (a total of 3240 observations). The Jenks natural breaks method was then used to the pooled dataset to calculate a common set of risk classification thresholds, which were consistently applied to classify risk levels for each year.

2.3.5. Spatial Autocorrelation Analysis

Spatial autocorrelation is used to characterize the degree to which geographic phenomena exhibit spatial clustering or dispersion [63]. In this study, global and local spatial autocorrelation of landscape risk at ancient sites were assessed using Global Moran's I and Local Indicators of Spatial Association (LISA), respectively, in ArcGIS Pro 3.0.2. Spatial weights were constructed using the K-nearest neighbors method with K = 8, and statistical significance was evaluated using 499 permutations at the 0.05 significance level. A positive and significant Moran's I indicates global spatial clustering, whereas a negative and significant value indicates spatial dispersion. A Moran's I value not significantly different from zero indicates the absence of significant global spatial autocorrelation [64]. LISA was used to identify local spatial clusters and spatial outliers [65]. Based on the local spatial association patterns, the results were classified into five types: High–High cluster (HH), Low–Low cluster (LL), High–Low outlier (HL), Low–High outlier (LH), and not significant (NS).

3. Results

3.1. Weights of the Indicator System

To ensure the comparability of risk assessment results across different years and minimize potential inconsistencies arising from year-specific weighting, the indicator data from the eight years were pooled into a single dataset. The entropy weight method was used to derive a common weight for each indicator, and these weights were consistently applied to the risk assessment for each year.

Based on the results of the indicator weight calculations (Table 5), the contributions of the three indicator layers to the overall weighting scheme differed considerably. Among these, the pressure layer accounts for the largest share of the composite weighting scheme. The state layer follows, and the response layer has the lowest. Within each indicator layer, indicator weights also varied substantially. Indicators with higher weights are primarily concentrated in the pressure and state layers, including slope, terrain undulation, population, as well as the PD, LSI, and DIVISION. Among these, population, PD, and terrain undulation had the three highest weights, constituting the core factors of the assessment system. In contrast, land cover has the lowest weight, suggesting a relatively limited contribution to the overall risk assessment.

Table 5. Assessment indicator weights.

Guideline	Element	Indicator	Weight
Pressure	Climate	Precipitation	0.04956
		Temperature	0.01281
	Geological	Terrain undulation	0.15528
		Slope	0.11337
	Human activities	Land cover	0.00883
		Population	0.21375
State	Environment	NDVI	0.02437
	Landscape pattern	LSI	0.13461
		DIVISION	0.1174
		PD	0.15575
Response	Preservation	Protection level	0.01427

3.2. Analysis of Spatio-Temporal Changes in Landscape Risks at Ancient Sites in Yuncheng City, 1990–2024

3.2.1. Risk Classification

Based on the landscape risk values of ancient sites in Yuncheng City from 1990 to 2024, this study employed the Jenks natural breaks classification method to establish a unified risk classification scheme and consistent grading thresholds. The risks were ultimately classified into five levels (1: very low risk; 2: low risk; 3: medium risk; 4: high risk; and 5: very high risk). The corresponding ranges of risk index values for each level are presented in Table 6.

Table 6. Risk classification thresholds.

Risk Level	Risk Description	Risk Value Range
1	Very low risk	0–0.1579
2	Low risk	0.1579–0.2044
3	Medium risk	0.2044–0.264
4	High risk	0.264–0.3545
5	Very high risk	0.3545–0.5367

3.2.2. Spatio-Temporal Distribution Characteristics of Landscape Risks at Ancient Sites

Figure 3 illustrates the distribution characteristics of landscape risk at ancient sites in Yuncheng City from 1990 to 2024. In terms of spatial distribution, risk levels across all periods in Yuncheng City exhibit strong spatial clustering, with a pattern characterized by "high risk at the periphery and low risk in the interior". Very-high-risk sites are primarily distributed in the mountain-plain transition zones, such as along the southern banks of the Yellow River, the northern foothills of the Zhongtiao Mountains, and the southern foothills of the Luliang Mountains in northern Yuncheng. Most very-high-risk sites are located at the interfaces of different landscape types, such as forest, farmland, and urban area, which are associated with more complex landscape configurations. High-risk and medium-risk sites are distributed around the very-high-risk sites, forming a gradual spatial transition toward low-risk areas. Low-risk sites were primarily distributed across the alluvial plain of the Yuncheng Basin. Low risk was the most widespread risk level in the study area, with contiguous farmland serving as the core landscape. Very-low-risk sites are mainly concentrated in the inland plain areas of Yuncheng, characterized by relatively homogeneous landscape types and higher landscape connectivity.

From 1990 to 2024, the spatial pattern of landscape risk at ancient sites in Yuncheng City remained generally stable. Very-high- and high-risk sites were consistently concentrated in the mountain–plain transition zones along the periphery of the study area, where multiple landscape types converge. Although their spatial locations and extents fluctuated slightly among years, the overall distribution pattern remained largely unchanged. Low-risk and very-low-risk sites remained concentrated in the plain areas throughout the study period, with relatively stable spatial locations and distribution ranges, and no obvious shifts in their spatial distribution were observed. Overall, during the study period, landscape risk associated with ancient sites exhibited relatively stable spatial differentiation, characterized by a concentration of high-risk sites in the peripheral areas and relatively low risk in the inland plain areas. This pattern indicates spatial heterogeneity in landscape risk across ancient sites under different landscape contexts.

3.2.3. Spatial Clustering Characteristics of Landscape Risks at Ancient Sites

To further reveal the spatial distribution patterns of landscape risks at ancient sites, Global Moran's I was used to assess the spatial autocorrelation of the risk assessment results from 1990 to 2024. The results show that the Moran's I index was positive for all years, with values of 0.35, 0.34, 0.34, 0.34, 0.34, 0.35, 0.33, and 0.37, respectively. This indicates that the landscape risk of ancient sites in Yuncheng City exhibits positive spatial correlation in its distribution, with a distinct pattern of spatial clustering. Overall, the relatively narrow range of Moran's I values (0.33–0.37) suggests that the spatial clustering pattern remained relatively stable over the study period.

Building on the global spatial autocorrelation identified by Moran's I, LISA analysis was further employed to identify local spatial clustering patterns, with the aim of clarifying the spatial differentiation characteristics of sites with different risk levels. As shown in Figure 4, the overall local clustering pattern of landscape risk remained highly stable from 1990 to 2024. In terms of spatial clustering zones, the High–High clusters were primarily distributed along the Yellow River in the peripheral areas of Yuncheng City and in the mountain-plain transition zone near the Zhongtiao Mountains. This distribution was largely consistent with the spatial distribution of high-risk sites described in the previous subsection, further reflecting the spatial clustering characteristic of high-risk sites. The spatial distribution of HH clusters remained generally stable throughout the study period, with changes occurring only in localized areas. For example, a small number of HH clusters emerged along the northern foothills of the Zhongtiao Mountains after 2020. In

contrast, the "Low–Low" clusters were primarily distributed in the inland plain areas of Yuncheng, particularly concentrated in regions with continuous agricultural landscapes, and maintained a high degree of stability across all periods.

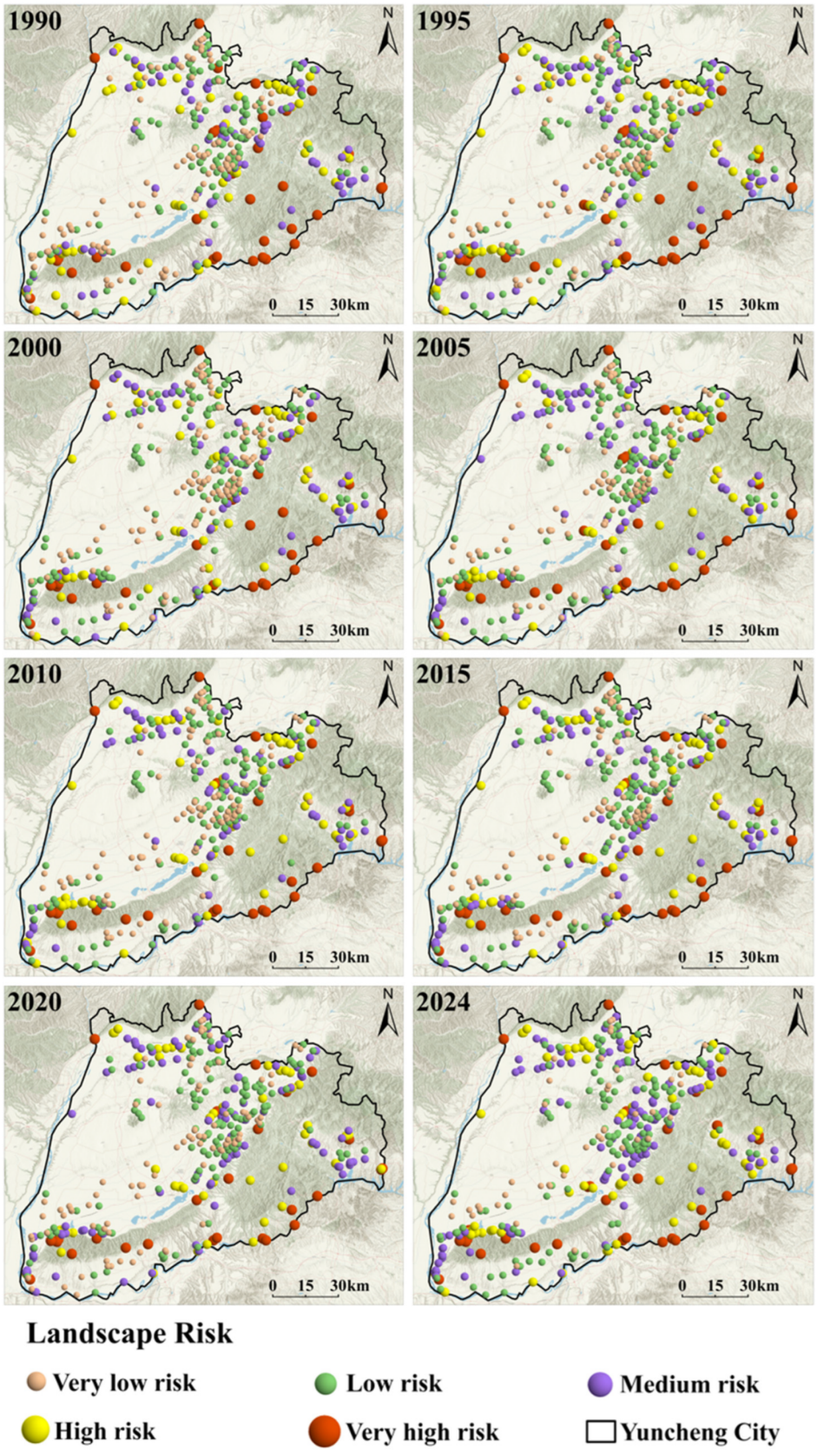


Figure 3. Landscape risk distribution at ancient sites in Yuncheng City.

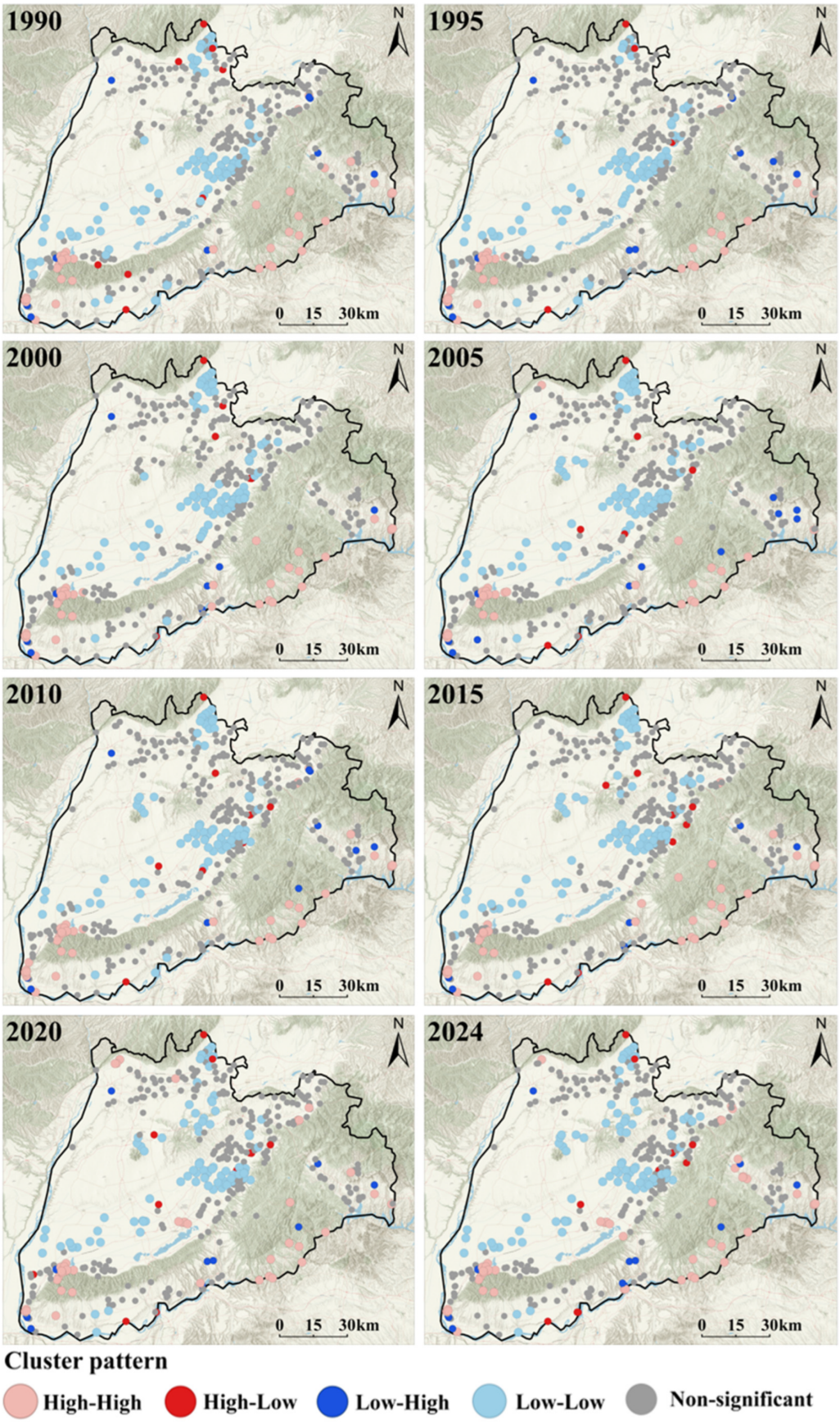


Figure 4. Local spatial autocorrelation clusters of landscape risks at ancient sites.

3.2.4. Changes in the Landscape Risk Classification Structure

Figure 5 illustrates the changes in the landscape risk structure and the number of ancient sites in Yuncheng City from 1990 to 2024. Overall, the landscape risk levels were predominantly classified as very low risk and low risk, accounting for more than 50% of all ancient sites throughout the study period. Among these, low risk level consistently represented the high proportion and was the primary landscape risk level in the study area.

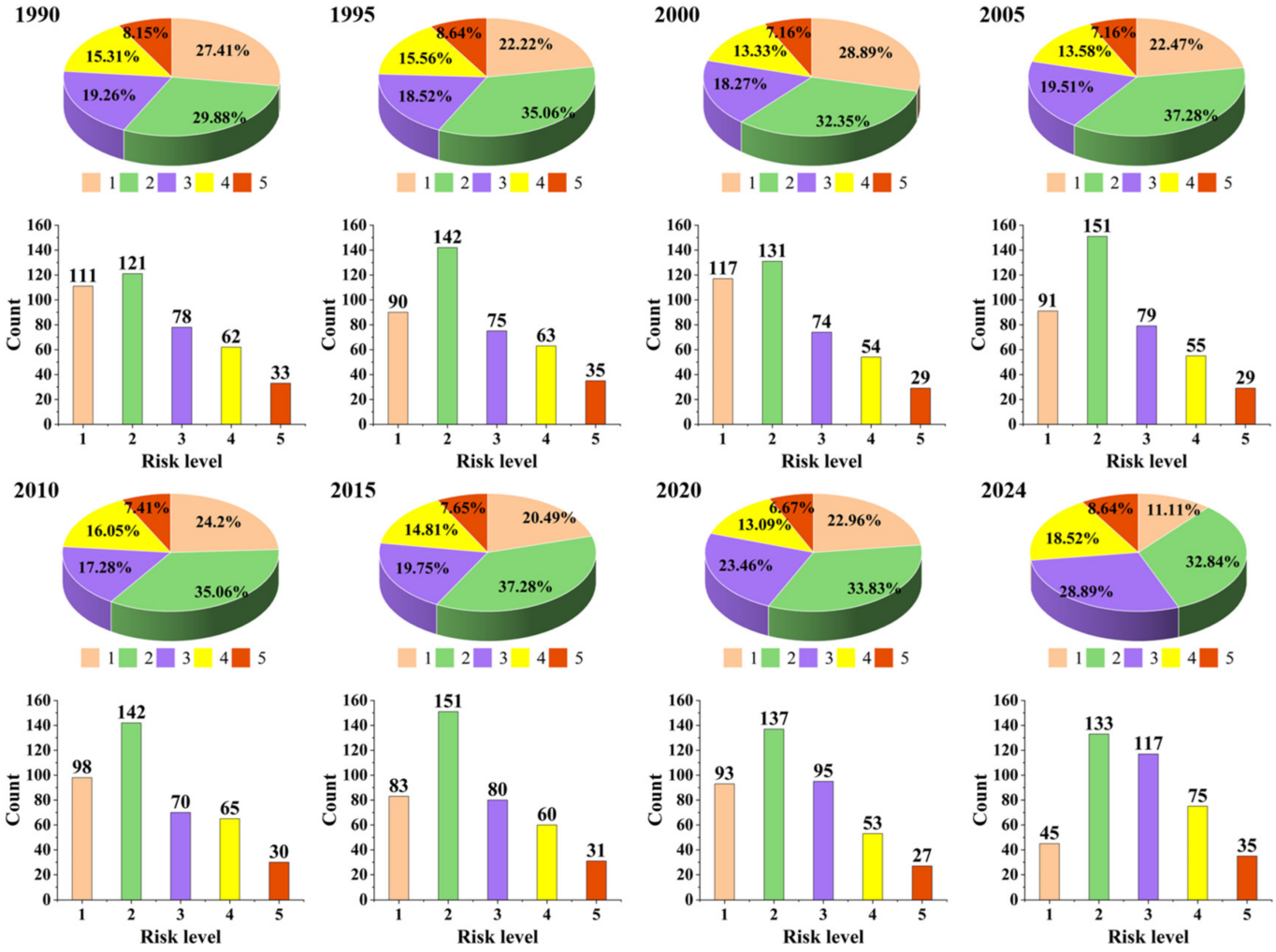


Figure 5. Statistical chart of landscape risks at ancient sites.

Note: Due to rounding to two decimal places, the percentages may have a cumulative deviation of ±0.02% from 100%.

In terms of the composition and temporal changes in risk levels, the risk structure of ancient-site landscapes in the study area underwent some changes from 1990 to 2024. From 1990 to 2000, the very low and low risk levels dominated the study area. The number of low-risk sites increased to a peak of 117 in 2000, accounting for 28.89% of the total. From 2000 to 2015, the number of very-low-risk sites continued to decline, whereas the number of low-risk sites increased, reaching a study-period peak of 151 in 2015, accounting for 37.28%. During the same period, the numbers of medium-, high-, and very-high-risk sites also showed slight increasing trends. From 2015 to 2024, the numbers of very-low- and low-risk sites generally declined. The number of very-low-risk sites fell to a study-period low of 45 in 2024 (11.11%). In contrast, the numbers of medium-, high-, and very-high-risk sites increased to varying degrees, reaching their respective study-period peaks of 117, 75,

and 35 sites in 2024. Overall, the risk structure of ancient-site landscapes gradually shifted from lower-risk toward medium- and higher-risk levels, suggesting a gradual increase in regional landscape risk.

In addition, a transition matrix was employed to quantify changes in landscape risk levels at ancient sites between adjacent periods (Figure 6). Overall, risk-level transitions occurred throughout the study period, but were predominantly confined to adjacent levels, with relatively few transitions spanning multiple risk levels. The most frequent transitions were bidirectional exchanges between the very-low and low risk levels and between the low and medium risk levels, which constituted the dominant transition patterns across the study periods. During 1990–2005, transitions were concentrated mainly between the very-low and low risk levels, with relatively few transitions from low to medium risk. During 2005–2020, transitions between low and medium risk became the dominant pattern. In contrast, during 2020–2024, the overall magnitude of transitions increased, accompanied by increases in the proportions of very-low-to-low, low-to-medium, and medium-to-high risk transitions. Collectively, these patterns suggest a gradual shift in the risk structure toward medium and higher risk levels during the later stage of the study period.

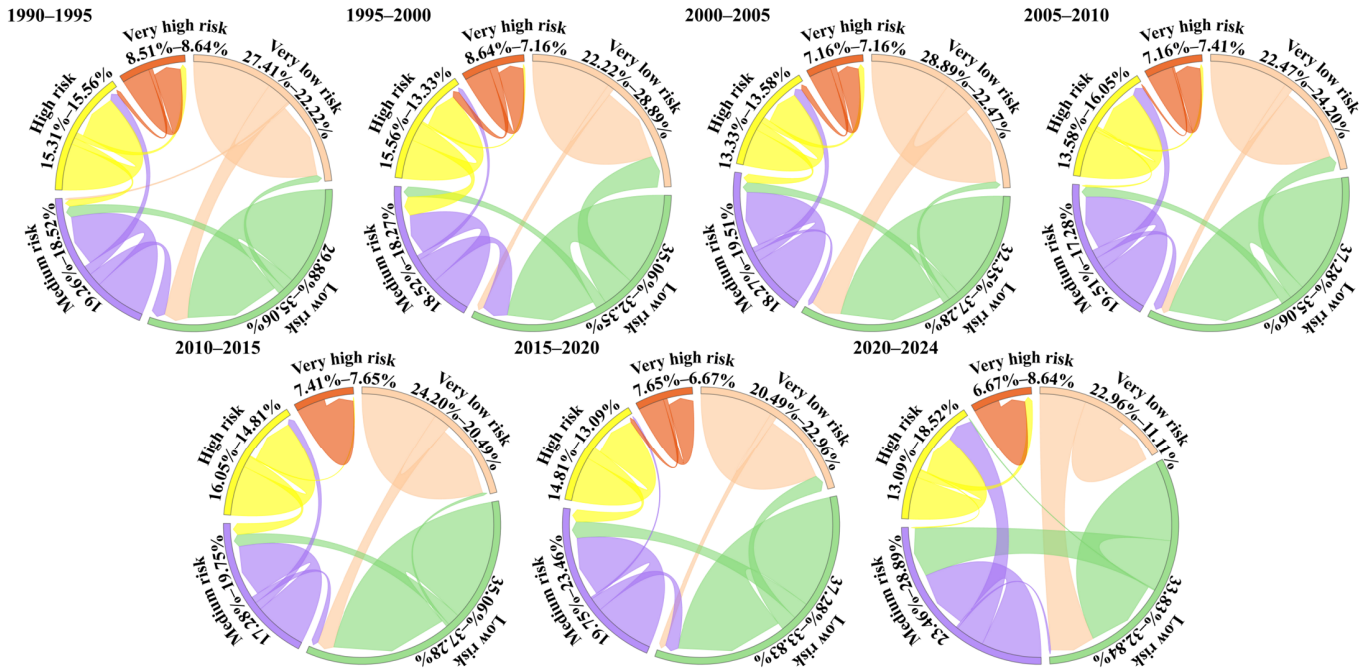


Figure 6. Conversion of different landscape risk levels.

4. Discussion

Most existing studies on landscape environmental risk assessment have focused on the regional-scale analyses, addressing issues such as sea-level rise [20], extreme climatic stressors [17], threats associated with urban expansion [21], landscape ecological risks [15,16], and environmental risks in arid regions [19]. However, comprehensive risk assessments at the scale of individual ancient sites and their surrounding landscapes remain relatively limited. Existing risk assessments at the landscape scale for ancient sites still rely heavily on a single land-use environmental factor [18], with insufficient consideration of the combined effects of natural environmental changes, human disturbance, and the state of site protection. From the perspective of the ancient-site landscape, this study constructed a landscape risk assessment system comprising 11 indicators based on the PSR framework and systematically assessed the landscape risks of ancient sites in Yuncheng City from 1990 to 2024. By analyzing their long-term evolution characteristics, the study revealed

the spatiotemporal heterogeneity, clustering patterns, and change processes of risk levels, thereby providing a basis for the protection and risk management of ancient site landscapes at the regional scale.

4.1. Analysis of Spatiotemporal Changes in Landscape Risks at Ancient Sites

The study found that the risk level of ancient site landscapes exhibits relatively stable spatial differentiation characteristics. This pattern may be closely related to regional variations in geomorphological features, intensity of human activities and land use structure in Yuncheng City. The mountain-plain transition zone is located in the transition area between different geomorphological units, with large topographic relief and slope [66]. Complex topography may exacerbate surface runoff and soil erosion processes, increasing the natural environmental pressure faced by the site landscape. Meanwhile, the region exhibits a complex distribution of agricultural land, forest land, and construction land, primarily characterized by spatial competition between construction and agricultural land, construction and forest land, as well as the intermingling and conversion between agricultural and forest land. With increasing urbanization and human activity, the degree of intermingling and fragmentation between construction land and surrounding agricultural and forest land may increase, leading to a more complex land use structure and further enhancing landscape fragmentation and anthropogenic disturbance. The intermingling of agricultural and forest land may also increase the frequency of land use conversion, impacting regional landscape stability. In summary, this region possesses both a complex natural topography and significant human disturbance, potentially exacerbating the instability of the regional landscape system and resulting in a higher landscape risk to ancient sites. In contrast, the central part of the basin is dominated by alluvial plains, with relatively flat terrain, a simpler landscape structure, and higher landscape connectivity [67], resulting in relatively low overall environmental pressure. Therefore, the spatial differentiation observed in this study is not merely a result of differences in the geographical locations of the sites, but may reflect regional risk characteristics arising from the combined effects of topographic conditions, human activities, and landscape patterns.

The results of the spatial autocorrelation analysis indicate that landscape risks at ancient sites in Yuncheng City exhibit significant clustering characteristics. This spatial clustering pattern may be related to regional differences in the natural geographic environment, land use patterns, and human activities. On the one hand, ancient sites with similar topographic, climatic, and ecological backgrounds often face comparable environmental pressures, and the vulnerability and risk levels of their landscape systems may also share certain similarities. On the other hand, population growth and urban development, which tend to exhibit pronounced spatial clustering [68], may expose adjacent ancient sites to similar anthropogenic disturbances, thereby contributing to spatial clustering of landscape risks. Meanwhile, the spatial clustering structure remained relatively stable overall during the study period, which may indicate that the regional natural geographic context and long-established land-use patterns exert certain constraints on the spatial distribution of landscape risks at ancient sites.

From a risk structure perspective, the landscape risks associated with ancient sites in Yuncheng City generally show a trend of evolving from low risk to medium-to-high risk. This change may be related to the intensified tourism development, urbanization, and changes in surrounding land use within the study area, consistent with previous studies on the impact of human activities on cultural heritage landscapes [69,70]. Risk levels primarily transition between adjacent levels, indicating that changes in risk levels tend to evolve gradually from the existing low risk level rather than through abrupt changes. Therefore, risk management for ancient site landscapes should not focus solely on high-risk areas

but should also pay attention to ongoing changes in risk levels in low-risk areas, thereby effectively preventing the deterioration of risks in ancient site landscapes.

4.2. Model Uncertainty and Sensitivity Analysis

4.2.1. Compatibility of Population Datasets

Population size serves as a key indicator of anthropogenic pressure, as population concentration reflects the intensity of potential human disturbance surrounding ancient sites. Due to the lack of long-term population datasets covering 1990 to 2024, this study integrated GlobPOP and LandScan datasets to characterize long-term population dynamics in the study area. However, GlobPOP and LandScan were generated using different modeling frameworks and population redistribution methods, resulting in certain differences in data sources and spatial distribution simulation approaches. Therefore, the integration of these two datasets may introduce uncertainty into the representation of population pressure, potentially affecting the accuracy and reliability of the resulting landscape risk assessment.

To assess the suitability and compatibility of two population datasets, this study selected the city of Yuncheng as the study area and conducted a pixel-level consistency analysis using 2020, the year in which the two datasets overlap. According to the results of the consistency analysis (Figure 7), the GlobPOP and LandScan population datasets exhibited a very strong linear correlation (Pearson's r = 0.99, $p < 0.05$). The regression equation is y = 0.96x + 18.54 (R^2 = 0.99), and the fitted line closely coincides with the 1:1 reference line (y = x). These results indicate a high degree of consistency between the two datasets in both spatial distribution and population magnitude. Although datasets differ in their data sources and modeling procedures, they exhibit a high degree of consistency in spatial representation at the regional scale. Therefore, at the regional scale, LandScan can serve as a supplementary data source for the GlobPOP time series.

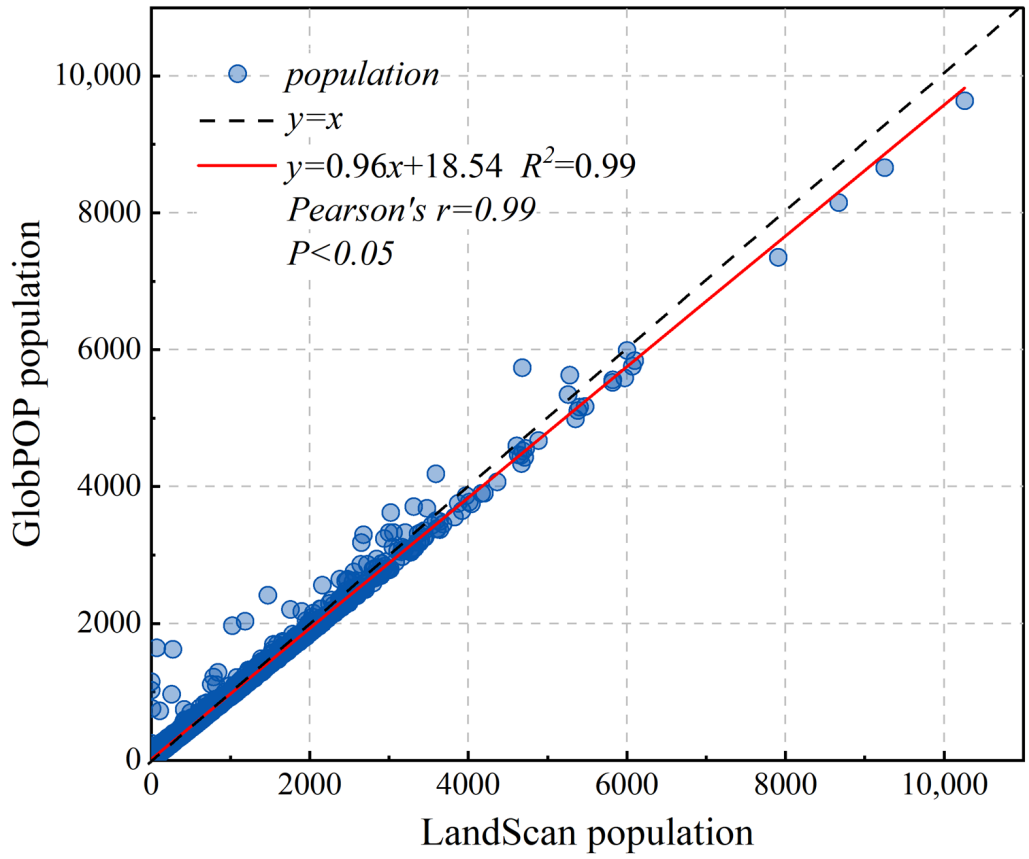


Figure 7. Consistency test for population data.

4.2.2. Sensitivity Analysis of Spatial Analysis Scale and Element Shape

The scale of spatial analysis and the shape of analysis units are key factors influencing the results of landscape risk assessments. Different analysis scales and spatial unit shapes may alter the spatial statistical characteristics of variables such as landscape pattern indicators and human activity pressures, thereby affecting the risk assessment results. To examine the sensitivity of the assessment results to the configuration of spatial analysis units, this study employed different minimum area thresholds (800,000 m^2 and 1,200,000 m^2), scale adjustment coefficients (k = 1.2, 1.8, 2.0), and analysis unit shapes. The consistency of the risk assessment results across these configurations was subsequently evaluated to assess the robustness of the proposed model.

The results of the sensitivity analysis of scale adjustment coefficients (Table 7) indicate that, compared with the baseline scenario (k = 1.5), the landscape risk assessment results under alternative coefficients generally maintain highly consistent. Across different scenarios, Spearman's correlation coefficients between the assessment results and the baseline scenario ranged from 0.957 to 0.978, while more than 78% of ancient sites retained the same risk category as in the baseline scenario. Further spatial stability testing of high-risk sites revealed that, under different scale adjustment coefficient scenarios, the overlap rate among the top 20% of high-risk sites exceeded 88.89%. This result indicates that although the scale adjustment coefficient alters the relative magnitude of the risk values of some sites, it does not change the main spatial identification results of high-risk sites.

Table 7. Sensitivity analysis result of scale adjustment coefficients.

Scenario	Scale Adjustment Coefficient (k)	Spearman Correlation Coefficient (ρ)	Number of Sites with Consistent Risk Classes	Percentage of Sites with Consistent Risk Classes (%)	The Overlap Rate of the Top 20% High-Risk Sites (%)
S1 (Baseline)	k = 1.5	1.000	405	100	100
S2	k = 1.2	0.969	317	78.27	95.06
S3	k = 1.8	0.978	343	84.69	91.36
S4	k = 2.0	0.957	322	79.51	88.89

The sensitivity analysis of different minimum area thresholds (Table 8) showed that the assessment results remained highly consistent with the baseline scenario after adjusting the minimum area threshold. Spearman's correlation coefficients between the assessment results and the baseline scenario were 0.988 and 0.991, respectively, and more than 90% of ancient sites retained the same landscape risk category as in the baseline scenario. These results demonstrate the high robustness of the assessment results to variations in the minimum area threshold. Furthermore, spatial stability analysis of high-risk sites showed that, under different scenarios, the overlap rate of the top 20% of high-risk ancient sites exceeded 93.83%. This finding indicates that changes in the minimum area threshold did not significantly alter the spatial identification characteristics of high-risk ancient sites.

Table 8. Sensitivity analysis result of minimum area thresholds.

Scenario	Minimum Landscape Analysis Area Threshold (m^2)	Spearman Correlation Coefficient (ρ)	Number of Sites with Consistent Risk Classes	Percentage of Sites with Consistent Risk Classes (%)	The Overlap Rate of the Top 20% High-Risk Sites (%)
S1 (Baseline)	1,000,000	1.000	405	100	100
S2	800,000	0.988	367	90.62	96.30
S3	1,200,000	0.991	365	90.12	93.83

In addition, a sensitivity analysis was conducted to evaluate the effect of analysis-unit shape on the risk assessment results by comparing circular and square analysis units. The results showed a high degree of consistency between the two configurations, with a

Spearman's correlation coefficient of 0.978. The risk levels of 341 ancient sites (84.20%) remained unchanged across the two configurations. Overall, the choice of analysis-unit shape had a limited influence on the risk assessment results, and the use of square analysis units did not substantially alter the spatial patterns or risk classifications of landscape risk at ancient sites.

4.2.3. Uncertainty in Ordinal Scoring

This study assigns risk scores ranging from 1 to 5 to different land-use types according to the potential intensity of associated human activities. However, different scoring schemes may alter the relative contribution of land-use indicators to the comprehensive risk index, thereby affecting the landscape risk assessment results. To examine the impact of land-use risk scoring schemes on assessment results, this study conducted a sensitivity analysis using different rankings of land-use types. In the baseline scenario, land-use types were assigned risk scores in descending order as follows: impervious surfaces: 5; cropland: 4; barren land: 3; grassland and shrub: 2; forest and water: 1. The sensitivity analysis results (Table 9) indicated that the assessment results under different scoring schemes show extremely high consistency with the baseline scheme, with Spearman's correlation coefficients all reaching 0.999. Furthermore, more than 98% of ancient sites retained the same landscape risk category as in the baseline scenario. These findings indicate that variations in the land-use risk scoring scheme have a minimal impact on the comprehensive landscape risk assessment results, suggesting that the model exhibits good robustness regarding the risk ranking of land-use types.

Table 9. Sensitivity analysis result of land-use scoring schemes.

Scenario	Land-Use Scoring Scheme	Spearman Correlation Coefficient (ρ)	Number of Sites with Consistent Risk Classes	Percentage of Sites with Consistent Risk Classes (%)
S1 (Baseline)	5-4-3-2-1	1.000	405	100
S2	5-4-5-2-1	0.999	405	100
S3	5-5-3-2-1	0.999	397	98.02
S4	5-3-4-2-1	0.999	404	99.75

4.3. Consistency Checks Based on Cases

To further evaluate whether the landscape risk assessment results are consistent with actual landscape changes, this study conducted a case-based consistency check using high-resolution imagery from Google Earth for two ancient sites. The results showed that changes in the risk levels of the two ancient sites were generally consistent with the observed changes in their surrounding landscapes within the corresponding landscape analysis units.

Taking the Anyì Ximenwai Site as an example, the high-resolution imagery (Figure 8) shows that the landscape analysis unit was characterized by relatively favorable ecological conditions in 2015, with farmland dominating the core area surrounding the site. By 2022, the expansion of construction land within the core area was evident, accompanied by a corresponding deterioration in the ecological conditions of the surrounding landscape. Consistent with these observed landscape changes, the assessed landscape risk level increased from "high risk" in 2015 to "very high risk" in 2024. This consistent correspondence provides supporting evidence that the assessment framework can capture changes in the surrounding landscape environment and reflect their associated changes in landscape risk.



Figure 8. Landscape changes for the Anyì Ximenwai Site.

The Sibeicunbei Site provides another example of the correspondence between observed landscape changes and the assessment results. As shown in Figure 9, in 2015, the landscape surrounding the site was dominated by farmland, with only a limited extent of built-up land. By 2024, built-up land had expanded substantially around the site, replacing a considerable portion of the original farmland and indicating intensified human disturbance. Consistent with these landscape changes, the site's landscape risk level increased from "medium risk" in 2015 to "high risk" in 2024. The parallel changes observed in land use and assessed risk suggest that the assessment results are broadly aligned with the actual evolution of the surrounding landscape.

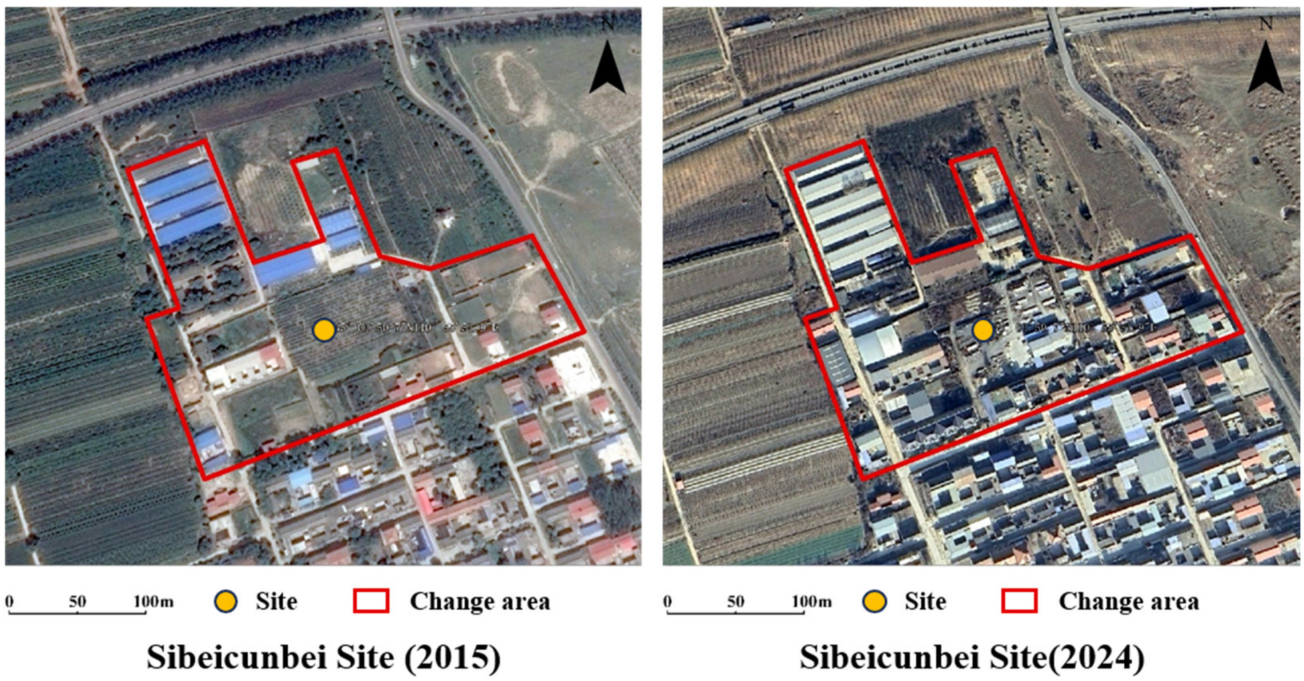


Figure 9. Landscape changes for the Sibeicunbei Site.

4.4. Recommendations for Sustainable

Based on the results of landscape risk assessment of ancient sites in Yuncheng City, this paper proposes the following recommendations from the perspective of sustainable development.

First, for areas with a high concentration of high-risk sites, conservation strategies should shift from site-specific protection toward coordinated regional conservation. When multiple high-risk sites form a "High–High" clusters, their risks may share common regional drivers. Therefore, for the mountain-plain transition zone—a region with a high concentration of high-risk sites—the high-risk sites and their surrounding landscapes within the region should be incorporated into an integrated regional conservation framework. The expansion of construction land and major land-use changes within the region should be strictly controlled to reduce the ongoing anthropogenic disturbance to the landscape environment of ancient sites and maintain the integrity of the region's overall landscape pattern.

Second, for sites experiencing sustained increases in risk, dynamic monitoring and preventive measures should be strengthened. For sites currently classified as low or medium risk but exhibiting persistent upward trends in risk, particular attention should be paid to changes in surrounding land use and landscape patterns. Potential risk factors, such as built-up land expansion and substantial land-use conversions, should be identified promptly, and targeted mitigation measures should be implemented accordingly. Such measures can help prevent the cumulative effects of localized landscape disturbances from causing further deterioration of the ancient-site landscape.

Finally, for areas where low-risk sites are concentrated and have remained stable over the long term, the primary focus should be on maintaining the status and providing moderate protection. In the low-risk site cluster in the inland plains of Yuncheng City, the existing contiguous agricultural landscape should be preserved to the greatest extent possible while accommodating agricultural production and regional development needs. The use of space at and around the sites should be reasonably planned to avoid unnecessary new construction and large-scale landscape alterations.

4.5. Research Limitations

Firstly, this study is subject to potential sample selection bias. Since sites lacking clear information on their protection levels were not included in the comprehensive assessment, the representativeness and generalizability of the findings to the broader population of ancient sites in Yuncheng City may be limited. The exclusion of unclassified sites from the study was primarily based on the following consideration: the absence of a formal protection classification does not necessarily indicate the lowest level of protection; simply assigning them the lowest protection value could introduce other forms of subjective bias. To ensure consistency in the interpretation of the protection response indicators, this study adopted a relatively conservative sample selection approach and excluded unclassified sites. In the future, we can further combine archival data and field survey data from cultural relics departments to supplement indicators such as the protection status and actual protection measures of all sites, and test the stability and applicability of the research results based on a more complete sample.

Secondly, the indicator system and the direction of risk indicators have several limitations. First, due to the lack of complete historical records of protection levels and their changes, this study used the institutional protection status of ancient sites recorded in the Third National Cultural Relics Survey and applied it to each assessment year. This approach makes it difficult to fully capture temporal changes in protection status and conservation measures during the study period. Future research could incorporate historical

records of changes in protection levels and dynamic protection management data to further improve the dynamic characterization of the response layer. Second, the indicator system characterizes risk primarily based on long-term climatic and topographic conditions, giving limited consideration to natural hazards such as extreme precipitation, landslides, and debris flows. Consequently, the current framework is more suitable for characterizing landscape risks associated with long-term natural environmental changes and human activities. Future research could construct hazard-sensitivity indicators based on historical disaster data, including extreme precipitation, floods, and landslides, to improve the ability of the risk assessment to capture the impacts of natural hazards. Third, this study treats annual mean temperature and total annual precipitation as positive indicators. While this simplification can characterize relative differences in regional climate pressure across different years, it may overlook the potential nonlinear and threshold effects of these factors on the landscape risk of ancient sites. Future research could incorporate nonlinear response models, threshold models, and other approaches to further identify the actual response relationships between temperature, precipitation, and the landscape risk of ancient sites.

Thirdly, this study only used the entropy weight method to determine the indicator weights. While this data-driven weighting method can reduce reliance on subjective judgment, it is difficult to fully reflect the actual role of indicators in the risk formation process. Future research could integrate expert knowledge with objective weighting methods through a combined subjective–objective weighting method, thereby improving the interpretability and mechanistic relevance of the indicator weights.

5. Conclusions

Based on the PSR framework, this study developed a landscape risk assessment method for ancient sites and used this method to systematically evaluate the landscape risks of ancient sites in Yuncheng City from 1990 to 2024. The main findings are as follows: (1) In terms of spatial distribution characteristics, the distribution of landscape risks for ancient sites in the study area exhibits significant spatial heterogeneity and a relatively stable pattern of spatial differentiation. Very-high-risk and medium-to-high-risk sites are primarily distributed in the foothill transition zone, where the terrain is fragmented and the ecosystem is relatively fragile. As a transitional zone between different landscape types, this area also experiences severe land-use conflicts, leading to a high level of landscape risk. Low-risk and very-low-risk sites are mainly distributed in the inland plain, which are characterized by relatively simple landscape structures and high connectivity, resulting in a lower risk level. The overall spatial distribution pattern remained largely unchanged throughout the study period, indicating a high degree of spatial stability in the landscape risks of ancient sites in Yuncheng City. (2) In terms of spatial clustering characteristics, the landscape risk of ancient sites in Yuncheng City exhibits significant positive spatial autocorrelation and strong spatial clustering. Global Moran's I remained positive and statistically significant throughout 1990–2024, ranging from 0.33 to 0.37, indicating a relatively stable positive spatial autocorrelation pattern. LISA analysis further reveals that High–High clusters were primarily distributed along the banks of the Yellow River and in the mountain-plain transition zones near the Zhongtiao Mountains, while Low–Low clusters were mainly concentrated in the inland plains and continuous agricultural landscapes of Yuncheng. This pattern was generally consistent with the overall spatial distribution of the risk levels. (3) In terms of the risk level structure, the overall landscape risk of ancient sites in Yuncheng City was predominantly low to medium, with very low and low risk levels accounting for a high proportion. Medium and higher risk levels were relatively rare but exhibited temporal fluctuations. Toward the end of the study, the number of medium-, high-, and very-high-risk sites increased, indicating an overall upward trend in landscape

risk. Risk level shifts primarily manifest as bidirectional changes between adjacent levels, with cross-level transitions occurring infrequently.

In summary, landscape risks at ancient sites in Yuncheng City exhibit distinct spatiotemporal variations, reflecting strong spatial heterogeneity and significant spatial clustering. Future research could be expanded in the following areas: first, refine the landscape risk assessment system for ancient sites by integrating data on dynamic conservation status, extreme weather events, and geological hazards. Second, simulate risk evolution under different development pathways by incorporating land use, population, and climate change scenarios. Third, conduct external validation using independent data such as field surveys, hazard inventories, and expert assessments. Fourth, potential driving factors such as urban boundary expansion and major infrastructure construction can be further incorporated to conduct an in-depth exploration of the driving mechanism of the spatiotemporal changes in the risk of ancient site landscapes. Finally, perform sensitivity analyses by varying weighting methods, key parameters, and analytical scales, and use uncertainty propagation methods to quantify the impact of uncertainties in weights, parameters, and other factors on the assessment results, thereby testing the model's robustness.

Author Contributions: Yinglian Gao: Writing—original draft, visualization, methodology, investigation, conceptualization, software, and data curation. Wei Hua: Writing—review and editing, supervision, and conceptualization. Beibei Zhao: Writing—review and editing, visualization, and software. Binhao Du: Writing—review and editing, visualization, and data curation. Zhenhua Gao: Supervision and data curation. Miaole Hou: Writing—review and editing, supervision, funding acquisition, and project administration. All authors have read and agreed to the published version of the manuscript.

Funding: This research was funded by the National Natural Science Foundation of China (No. 42171444).

Data Availability Statement: The ancient sites data used in this study were obtained from Shanxi Provincial Research Institute of Archaeology and are available from the authors with the permission of Shanxi Provincial Research Institute of Archaeology. Other raw data supporting the conclusions of this article will be made available by the authors on request.

Conflicts of Interest: The authors declare no conflicts of interest.

References

1. United Nations. Convention Concerning the Protection of the World Cultural and Natural Heritage. Available online: https://www.un.org/zh/documents/treaty/whc (accessed on 14 April 2026).
2. Yang, X. Construction, Application and Thinking of Virtual Simulation Experiment of Field Archaeological Excavation. Master's Thesis, Zhengzhou University, Zhengzhou, China, 2021.
3. ICOMOS. Xi'an Declaration-Conservation of the Setting of Heritage. Available online: https://construct-vision.org/charter/xian-declaration-on-the-conservation-of-the-setting-of-heritage-structures-sites-and-areas/ (accessed on 13 August 2026).
4. Antoniou, A.; Tsegas, G.; Moussiopoulos, N.; Theodossiou, N. Assessment of the Impacts of Climate Change on a World Heritage Site in Greece. *J. Cult. Herit.* **2025**, *73*, 498–509. [CrossRef]
5. Gambilongo, L.; Chieffo, N.; Lourenço, P.B. A Comprehensive Approach to Assess the Seismic Vulnerability of Archaeological Sites: The Wupatki Pueblo in Arizona. *Bull. Earthq. Eng.* **2024**, *22*, 4413–4445. [CrossRef]
6. Nastou, M.P.P.; Zerefos, S.C. Effects of Climate Change on Open Air Heritage: A Review and the Situation in the Region of Mediterranean. *Herit. Sci.* **2024**, *12*, 367. [CrossRef]
7. Forti, L.; Brandolini, F.; Oselini, V.; Peyronel, L.; Pezzotta, A.; Vacca, A.; Zerboni, A. Geomorphological Assessment of the Preservation of Archaeological Tell Sites. *Sci. Rep.* **2023**, *13*, 7683. [CrossRef]
8. Papageorgiou, N.; Hadjimitsis, D.; Danezis, C.; Lasaponara, R. Assessment of Soil Erosion Risk in Cultural Heritage Sites: A Bibliometric Analysis. *Heritage* **2025**, *8*, 307. [CrossRef]
9. AlHaddad, M.; Arar, M.; Alhammad, R. Toward Sustainable Urban Growth: Spatial Modeling for the Impact of Cultural and Natural Heritage on City Growth and Their Role in Developing Sustainable Tourism. *Alex. Eng. J.* **2023**, *69*, 639–676. [CrossRef]

10. Butt, N.U.S.Z.; Wang, X.; Luo, L.; Ul Hussan, H. Evaluating the Impact of Urban Encroachment and Land Cover Changes on World Cultural Heritage Site Taxila: A Spatio-Temporal Analysis from 1990 to 2024. *Sustainability* **2025**, *17*, 1059. [CrossRef]
11. Chen, J.; Zhang, Y.; Liu, X.; Sun, X. Analysis of Spatial-Temporal Evolution of Landscape Patterns in Ancient Large City-Sites Based on Multi-Temporal Landsat Imagery: A Case Study of the Zhouyuan Site Region in China. *Eur. J. Remote Sens.* **2022**, *55*, 471–484. [CrossRef]
12. Liu, H.; Chen, F.; Liao, Y. Remote sensing dynamic monitoring and driving factor analysis for the Beijing section of Ming Great Wall. *Remote Sens. Nat. Resour.* **2023**, *35*, 255–263.
13. Wang, C.; Xu, D.; Lin, W. Remote sensing monitoring and land cover change of the world cultural landscape heritage in Honghe Hani Terrace, China. *Ecol. Environ. Sci.* **2021**, *30*, 233–241. [CrossRef]
14. Kim, J.; Choi, H.; Shin, W.; Yun, J.; Song, Y. Complex Spatiotemporal Changes in Land-Use and Ecosystem Services in the Jeju Island UNESCO Heritage and Biosphere Site (Republic of Korea). *Environ. Conserv.* **2022**, *49*, 272–279. [CrossRef]
15. Chen, X.; Yang, Z.; Wang, T.; Han, F. Landscape Ecological Risk and Ecological Security Pattern Construction in World Natural Heritage Sites: A Case Study of Bayinbuluke, Xinjiang, China. *ISPRS Int. J. Geo-Inf.* **2022**, *11*, 328. [CrossRef]
16. Du, J.; Bi, S.; Zhang, Y.; Chen, M. Landscape Ecological Risk Assessment and Driving Factors in Guyi Basin Cultural Heritage Sites: A Multi-Scenario Simulation Perspective. *npj Herit. Sci.* **2026**, *14*, 36. [CrossRef]
17. Canesi, L.; Sardella, A.; Vogler, R.; Kaiser, A.; Vaccaro, C.; Bonazza, A. Hazard Analysis and Vulnerability Assessment of Cultural Landscapes Exposed to Climate Change-Related Extreme Events: A Case Study of Wachau (Austria). *Heritage* **2024**, *7*, 1917–1934. [CrossRef]
18. Li, W.; Yang, R.; Yan, L.; Xie, Y.; Liu, H.; Chen, F. Risk Assessment of City Site Landscapes in the Central Plains of China. *Herit. Sci.* **2023**, *11*, 14. [CrossRef]
19. Zhang, S.; Yang, Z.; Wang, C. Environmental Risk Assessment of Earthen Heritage Sites in Arid Regions: A Case Study of the Great Wall in Xinjiang. *npj Herit. Sci.* **2025**, *13*, 200. [CrossRef]
20. Zengin, E. Inundation Risk Assessment of Eastern Mediterranean Coastal Archaeological and Historical Sites of Türkiye and Greece. *Env. Monit. Assess.* **2023**, *195*, 968. [CrossRef]
21. Sartori Peruzzo, R.; Valdati, J.; McHenry, M. Land Tenure and Future Development Affect Integrity and Geodiversity in Brazilian Indigenous Geocultural Sites. *Geomorphology* **2025**, *481*, 109770. [CrossRef]
22. Rapport, D.; Friend, A. *Towards a Comprehensive Framework for Environmental Statistics: A Stress-Response Approach*; Catalogue No. 11-510; Statistics Canada: Ottawa, ON, Canada, 1979.
23. Zhou, B.; Xu, J.; Yu, H.; Wang, L. Comprehensive Assessment of Ecological Risks of Island Destinations—A Case of Mount Putuo Island, China. *Ecol. Indic.* **2023**, *154*, 110783. [CrossRef]
24. Hu, N.; Wang, G.; Ma, Z.; Zhao, M.; Yuan, Y.; Zhang, T.; Chen, Q.; Meng, J.; Wang, J. Multi-Scenario Simulation of Land Use Dynamics and Ecological Risk: A Case Study of the Liaohe Estuary National Wetland Reserve Using PLUS-Markov and PSR Models. *Front. Environ. Sci.* **2024**, *12*, 1361970. [CrossRef]
25. Wu, D.; Chen, T.; Zhang, L.; Ling, H.; Yang, J.; Shen, C. Ecological Risk Assessment under the PSR Framework and Its Application to Shallow Urban Lakes. *Environ. Sci. Pollut. Res.* **2024**, *31*, 23568–23578. [CrossRef]
26. Yang, J.; Zheng, J.; Han, C.; Lu, B.; Yu, W.; Wang, Z.; Wu, J.; Han, L. Exploring Suitable Models for Regional Ecological Development: A Study on Multi-Scenario Ecological Risk Assessment in Typical Arid Regions. *Land Degrad. Dev.* **2025**, *36*, 2815–2830. [CrossRef]
27. Xu, M.; Huang, X.; Li, J.; Qi, S.; Zhang, Y.; Zhang, X. Assessing the Ecological Risk and Its Driving Forces on Islands Using the Pressure-State-Response Model. *Sci. Rep.* **2025**, *15*, 23162. [CrossRef]
28. Lai, S.; Sha, J.; Eladawy, A.; Li, X.; Wang, J.; Kurbanov, E.; Lin, Z.; Wu, L.; Han, R.; Su, Y.-C. Evaluation of Ecological Security and Ecological Maintenance Based on Pressure-State-Response (PSR) Model, Case Study: Fuzhou City, China. *Hum. Ecol. Risk Assess. Int. J.* **2022**, *28*, 734–761. [CrossRef]
29. Sun, X.; Peng, B.; Elahi, E.; Wan, A. Examining the Evolution and Influential Factors of Regional Ecological Security Patterns: A Case Study of Jiangsu Province, China. *Stoch. Environ. Res. Risk Assess.* **2025**, *39*, 999–1013. [CrossRef]
30. Chamani, R.; Sadeghi, S.H.; Zare, S.; Shekohideh, H.; Mumzaei, A.; Amini, H.; Hemmati, L.; Zarei, R. Flood-Oriented Watershed Health and Ecological Security Conceptual Modeling Using Pressure, State, and Response (PSR) Approach for the Sharghonj Watershed, South Khorasan Province, Iran. *Nat. Resour. Model.* **2024**, *37*, e12385. [CrossRef]
31. Boori, M.S.; Choudhary, K.; Paringer, R.; Kupriyanov, A. Eco-Environmental Quality Assessment Based on Pressure-State-Response Framework by Remote Sensing and GIS. *Remote Sens. Appl. Soc. Environ.* **2021**, *23*, 100530. [CrossRef]
32. Halder, S.; Das, S.; Bose, S. Environmental Risk Analysis of a Ramsar Site: A Case Study of East Kolkata Wetlands with PSR Framework. *Environ. Monit. Assess.* **2024**, *196*, 432. [CrossRef]
33. Wang, Q.; Li, S.; Li, R. Evaluating Water Resource Sustainability in Beijing, China: Combining PSR Model and Matter-Element Extension Method. *J. Clean. Prod.* **2019**, *206*, 171–179. [CrossRef]

34. Zhong, Q.; Dong, T. Exploring the Spatiotemporal Trends and Influencing Factors of Human Settlement Suitability in Hunan Province Traditional Villages. *Sci. Rep.* **2024**, *14*, 25319. [CrossRef]
35. Fu, L.; Ding, M.; Zhang, Q. Flood Risk Assessment of Urban Cultural Heritage Based on PSR Conceptual Model with Game Theory and Cloud Model—A Case Study of Nanjing. *J. Cult. Herit.* **2022**, *58*, 1–11. [CrossRef]
36. Bai, H.; He, L.; Cao, X.; Wang, M.; Liu, J.; Ma, Y.; Jing, R.; Jiang, L. An Integrated DPSIR-Extension Cloud Model Framework for Assessing Typhoon Risk to Coastal Architectural Heritage. *npj Herit. Sci.* **2026**. [CrossRef]
37. Yuncheng Municipal People's Government. Natural Geographical Environment. Available online: https://www.yuncheng.gov.cn/doc/2021/05/06/123127.shtml (accessed on 14 April 2026).
38. Chen, J.; Hu, J.; Zhao, L.; Du, H. Comprehensive Performance Comparison and Evaluation of High-Quality Wheat Varieties under Ecological Conditions in Yuncheng City. *Seed Sci. Technol.* **2026**, *44*, 5–8. [CrossRef]
39. Sun, P.; Zhang, M.; Zhang, J.; Cheng, X.; Zhu, L.; Xue, Q.; Wang, J. Geo-hazards Research and Investigation in the Loess Regions of Western China. *Northwest. Geol.* **2022**, *55*, 96–107. [CrossRef]
40. Cai, Y.; Li, X.; Zhu, P.; Nie, S.; Wang, C.; Liu, X.; Chen, Y. China Earth Observation Data Cube: The 30-m Seamless Annual Leaf-On Landsat Composites from 1985 to 2023. *J. Remote Sens.* **2025**, *5*, 0698. [CrossRef]
41. Peng, S.; Ding, Y.; Liu, W.; Li, Z. 1 km Monthly Temperature and Precipitation Dataset for China from 1901 to 2017. *Earth Syst. Sci. Data* **2019**, *11*, 1931–1946. [CrossRef]
42. Yang, J.; Huang, X. The 30 m Annual Land Cover Datasets and Its Dynamics in China from 1985 to 2024. *Zenodo* **2025**. [CrossRef]
43. Liu, L.; Cao, X.; Li, S.; Jie, N. GlobPOP: A 33-Year (1990–2022) Global Gridded Population Dataset Generated by Cluster Analysis and Statistical Learning 2024. *Zenodo* **2024**. [CrossRef]
44. Lebakula, V.; Gonzales, J.; Stipek, C.; Tsybina, E.; Zimmer, A.; Nukavarapu, N.; Jeong, B.; Reynolds, B.; Kaufman, J.; Fan, J.; et al. *LandScan Global 2024*; Oak Ridge National Laboratory (ORNL): Oak Ridge, TN, USA, 2025.
45. Geospatial Data Cloud. Available online: https://www.gscloud.cn/search (accessed on 7 August 2026).
46. Colette, A. *Climate Change and World Heritage: Report on Predicting and Managing the Impacts of Climate Change on World Heritage and Strategy to Assist States Parties to Implement Appropriate Management Responses*; UNESCO World Heritage Centre: Paris, France, 2007.
47. Yang, Y.; Zhang, C.; Zhang, J.; Wang, Y. Changes in soil moisture and dryness and their response to climate change in the Guanzhong region. *Arid. Zone Res.* **2024**, *41*, 261–271. [CrossRef]
48. Gao, M.; Li, Y.; Zhang, X.; Zhang, F.; Liu, B.; Gao, S.; Chen, X. Influence of freeze-thaw process on soil physical, chemical and biological properties: A review. *J. Agro-Environ. Sci.* **2016**, *35*, 2269–2274.
49. Holz, D.J.; Williard, K.W.J.; Edwards, P.J.; Schoonover, J.E. Soil Erosion in Humid Regions: A Review. *J. Contemp. Water Res. Educ.* **2015**, *154*, 48–59. [CrossRef]
50. Zhao, Y.; Zhu, D.; Wu, Z.; Cao, Z. Extreme Rainfall Erosivity: Research Advances and Future Perspectives. *Sci. Total Environ.* **2024**, *917*, 170425. [CrossRef]
51. Zhao, J.; Wang, Z.; Dong, Y.; Yang, Z.; Govers, G. How Soil Erosion and Runoff Are Related to Land Use, Topography and Annual Precipitation: Insights from a Meta-Analysis of Erosion Plots in China. *Sci. Total Environ.* **2022**, *802*, 149665. [CrossRef]
52. Tong, Q.; Qiu, F. Population Growth and Land Development: Investigating the Bi-Directional Interactions. *Ecol. Econ.* **2020**, *169*, 106505. [CrossRef]
53. Zhang, T.; Sun, Y.; Guan, M.; Kang, J.; Zhang, B. Human Activity Intensity in China under Multi-Factor Interactions: Spatiotemporal Characteristics and Influencing Factors. *Sustainability* **2022**, *14*, 3113. [CrossRef]
54. Wang, H.; Song, C. Regional ecological risk assessment of wetlands in the Sanjiang Plain. *Prog. Geogr.* **2019**, *38*, 872–882.
55. Zhang, X.; Song, J.; Wang, Y.; Sun, H.; Li, Q. Threshold Effects of Vegetation Coverage on Runoff and Soil Loss in the Loess Plateau of China: A *Meta*-Analysis. *Geoderma* **2022**, *412*, 115720. [CrossRef]
56. Li, J.; Chen, Y.; Yao, X.; Chen, A. Risk Management Priority Assessment of Heritage Sites in China Based on Entropy Weight and TOPSIS. *J. Cult. Herit.* **2021**, *49*, 10–18. [CrossRef]
57. National Cultural Heritage Administration. Law of the People's Republic of China on Cultural Relics Protection. Available online: http://www.ncha.gov.cn/art/2024/11/9/art_2301_42898.html (accessed on 28 May 2026).
58. Ministry of Personnel of the People's Republic of China; National Cultural Heritage Administration. National Administrative Measures of Specific Funds for the Protection of Cultural Relics. Available online: https://www.gov.cn/zhengce/zhengceku/202402/content_6930151.htm (accessed on 28 May 2026).
59. Qu, W.; Li, J.; Song, W.; Li, X.; Zhao, Y.; Dong, H.; Wang, Y.; Zhao, Q.; Qi, Y. Entropy-Weight-Method-Based Integrated Models for Short-Term Intersection Traffic Flow Prediction. *Entropy* **2022**, *24*, 849. [CrossRef]
60. Li, F.; Li, D. Combination Evaluation Model Based on Entropy Weight Method. *Inf. Technol. Informatiz.* **2021**, 148–150. [CrossRef]
61. Zhao, L.; Li, Q.; Jin, W.; Zhang, C.; Xuan, X. The change characteristics of eco-environment in the Yellow River wetland nature reserve based on entropy weights. *J. Henan Norm. Univ. (Nat. Sci. Ed.)* **2026**, *54*, 47–54. [CrossRef]
62. Ying, X.; Wu, C.; Jia, Y.; Meng, Q.; Ma, S.; Liao, J. Research on Multi-Model Grading Optimization of Landslide Susceptibility Driven by Machine Learning: A Case Study of Lixian County, Sichuan Province. *Geoscience* **2026**, *40*, 263–274. [CrossRef]

63. Chen, Y.; Shi, H.; Zhu, P.; Qiao, Z. Spatiotemporal dynamics and applicability assessment of two vegetation indices for typical plant communities in the three-river headwaters region. *Acta Ecol. Sin.* **2026**, *46(22)*. [CrossRef]
64. Lin, X.; Wang, Z. Landscape Ecological Risk Assessment and Its Driving Factors of Multi-Mountainous City. *Ecol. Indic.* **2023**, *146*, 109823. [CrossRef]
65. Anselin, L. Local Indicators of Spatial Association—LISA. *Geogr. Anal.* **1995**, *27*, 93–115. [CrossRef]
66. Bai, W.; He, Z.; Tan, Y.; Robinson, G.M.; Zhang, T.; Wang, X.; He, L.; Li, L.; Wu, S. Vegetation Classification in a Mountain–Plain Transition Zone in the Sichuan Basin, China. *Land* **2025**, *14*, 184. [CrossRef]
67. Vagge, I.; Sgalippa, N.; Chiaffarelli, G. Agricultural Landscapes: A Pattern-Process-Design Approach to Enhance Their Ecological Quality and Ecosystem Services through Agroforestry. *Diversity* **2024**, *16*, 431. [CrossRef]
68. Zhou, Y.; Li, X.; Liu, Y. Land Use Change and Driving Factors in Rural China during the Period 1995-2015. *Land Use Policy* **2020**, *99*, 105048. [CrossRef]
69. Żemła-Siesicka, A. Tourism Landscape Footprint in the Archaeological Landscape. *Environ. Impact Assess. Rev.* **2023**, *103*, 107255. [CrossRef]
70. Fu, L.; Zhang, Q.; Tang, Y.; Pan, J.; Li, Q. Assessment of Urbanization Impact on Cultural Heritage Based on a Risk-Based Cumulative Impact Assessment Method. *Herit. Sci.* **2023**, *11*, 177. [CrossRef]

Disclaimer/Publisher's Note: The statements, opinions and data contained in all publications are solely those of the individual author(s) and contributor(s) and not of MDPI and/or the editor(s). MDPI and/or the editor(s) disclaim responsibility for any injury to people or property resulting from any ideas, methods, instructions or products referred to in the content.